Biosensors and Bioelectronics 139 (2019) 111296

Contents lists available at ScienceDirect

Biosensors and Bioelectronics

journal homepage: www.elsevier.com/locate/bios

Towards ultra-wide operation range and high sensitivity: Graphene film based pressure sensors for fingertips

Ziyu Yue, Xingke Ye, Shihong Liu, Yucan Zhu, Hedong Jiang, Zhongquan Wan, Yuan Lin, Chunyang Jia*

State Key Laboratory of Electronic Thin Films and Integrated Devices, School of Electronic Science and Engineering, University of Electronic Science and Technology of China, Chengdu, 610054, PR China

ARTICLE INFO

Keywords:
Pressure sensor
Graphene film
Wide range
High sensitivity
Electronic skin

ABSTRACT

Remarkable research efforts have been devoted to replicate the tactile sensitivity of human skin. Unfortunately, so far flexible pressure sensors reported barely fit the tactile requirements for fingertips, which could endure a pressure over 100 kPa and also can sense a gentle touch. It is vital to develop flexible pressure sensors which can ensure high sensitivity and wide operation range simultaneously, to satisfy the demands of mimicking the pressure sensing function of fingertips. In this work, a mini-size, light-weight but high-performance graphene film based pressure sensor is presented. Owing to the advanced structure with fluctuations on surface and fluffy-layered structure in cross-section of the graphene film, this pressure sensor shows an extraordinary performance of high sensitivity of 10.39 kPa^{-1} (0–2 kPa), ultra-wide operation range up to 200 kPa, impressively stable repeatability, high working frequency, rapid response and recovery time. Moreover, the demonstrated results of the detection of traditional Chinese medicine wrist-pulse waveform and the bionic fingertip tactile sensors, suggest the great application potential of the obtain device in biomedical field and bionic skins field.

1. Introduction

Our lives are becoming smarter than ever before due to the rapid development of wearable electronics in last few decades, which substantially increased the experiences of human-machine interactions. Sensors with the function of transferring any other physical quantities to electronic quantities, are the keys of practical applications of wearable electronics such as electronic skins (Kim et al., 2018; Lai et al., 2016; Shi et al., 2016; Wu and Haick, 2018; Zang et al., 2015; Zhao and Zhu, 2017), wearable health monitors (Gao et al., 2016; Kim et al., 2016; Kuila et al., 2011; Morales-Narvaez et al., 2017), and portable entertainment equipment (Chou et al., 2015; Park et al., 2017). For tactile sensitivity, flexible pressure sensors have attracted vast attention of researchers due to their flexibility, high-performance, light weight, and integration possibility (Ge et al., 2018; Lipomi et al., 2011; Liu et al., 2017; Nesser et al., 2018; Schwartz et al., 2013; Wang et al. 2017, 2018). Comparing with others pressure sensing mechanisms, the piezoresistive sensors show advantages in extraordinary performance, ease of fabrication, direct measurement and low energy consumption (Jian et al., 2017; Li et al., 2015; Pan et al., 2014; Yao et al., 2013).

For pressure sensors, performance of high sensitivity along with wide operation range is commonly desired. In order to meet the expected piezoresistive performance, so far researchers have presented various type of flexible pressure sensors based on different materials such as conductive polymer (Lai et al., 2016; Mannsfeld et al., 2010; Pan et al., 2014; Zhang et al., 2018a), gold nanowires (Gong et al., 2014; Nesser et al., 2018), carbon nanotubes (Jian et al., 2017; Lipomi et al., 2011; Yamada et al., 2011) and graphene (Chen et al., 2018; Ge et al., 2018; Liu et al., 2017; Park et al., 2018; Sheng et al., 2015; Tao et al., 2017; Yao et al., 2013). Despite diverse substrates, the mechanisms of piezoresistive is the same: the conductivity of material will change with the variation of contact area under the influence of applied pressure (Tao et al., 2017). Therefore, to optimize the performances of pressure sensors such as sensitivity, operation range, durability, response and recovery time, the modification for variation degree of the contact area or the microstructure of material, is essential. Sheng et al. introduced bubble-decorated honeycomb-like graphene films pressure sensor which showed an ultrahigh sensitivity of 161.6 kPa^{-1} (Sheng et al., 2015). Jian et al. fabricated a pressure sensor based on aligned carbon nanotubes/graphene and micro-structured polydimethylsiloxane with a high sensitivity of 19.8 kPa^{-1} (Jian et al., 2017). Tian et al. demonstrated face-to-face laser-scribed graphene

* Corresponding author.
E-mail address: cyjia@uestc.edu.cn (C. Jia).

https://doi.org/10.1016/j.bios.2019.05.001
Received 18 February 2019; Received in revised form 20 April 2019; Accepted 1 May 2019
Available online 07 May 2019
0956-5663/

pressure sensor which achieved a large range of 113 kPa (Tian et al., 2015). Liu et al. introduced a graphene-silk network pressure sensor with a large operation range of 140 kPa (Liu et al., 2017). Based on these researches, it is obvious that graphene possesses great potential in high-performance pressure sensors due to the excellent conductivity, high mechanical stability and light weight properties (Chen et al., 2018). More importantly, graphene could be easily produced to form conductive microstructures. It had already been reported that graphene can be used to cover internal lining of porous or gaps of material, such as paper (Tao et al., 2017), silk (Liu et al., 2017), and polyurethane sponge (Yao et al., 2013). Unfortunately, so far there is no perfect material has been reported with both high sensitivity and wide operation range. Hence the tradeoff among those performance features according to their application is crucial for pressure sensors. For instance, fingertips are the most sensitive part of human body which can sense pressure of over 100 kPa along with tremendous tactile sensitivity. Therefore, it is urgently necessary for flexible pressure sensor that have wide operation range and high sensitivity simultaneously, to satisfy the demands of mimicking the pressure sensing function of fingertips.

Herein, we introduce a flexible pressure sensor based on graphene film with high sensitivity and wide operation range. By employing in-situ chemical reduction method and eco-friendly reducing agent Vitamin C, this free-standing graphene film (GF) presented fluctuations on surface and fluffy-layered structure in cross-section. Owing to this advanced structure of GF, the graphene film based pressure sensor (GFPS) presents impressive performance of high sensitivity of 10.39 kPa^{-1} (< 2 kPa) along with extraordinarily ultra-wide operation range up to 200 kPa. Moreover, the GFPS illustrates a rapid response time of 11.6 ms and a high working frequency of 6 Hz. Meanwhile, we also demonstrate some applications of the obtained pressure sensor in biomedical field and bionic skins, showing the great applicable potential of flexible pressure sensor for highly innovative and smart future applications.

2. Materials and methods

Fig. 1a presents the complete fabrication process of GFPS. Firstly, the mixture of graphene oxide suspension and Vitamin C was dropped into Teflon tray and heated in oven, and the in-situ chemical reduction process reduced graphene oxide and assembled to film simultaneously. Then, the GF was peeled off from Teflon tray, and cut into proper size and placed between two stripe-shape of press-to-flat foam-nickel electrodes. After packaged by polyethylene terephthalate (PET) film, the flexible GFPS is obtained. More detailed information shows in Experimental section in supplemental information. Importantly, this mini-size of 1.5 × 1.5 mm^2 operation area and ultra-light of 0.047 g weight GFPS is perfectly suitable for fingertips pressure sensors.

3. Results and discussion

3.1. Material characterization

For skin-contacting wearable devices, we used in-situ chemical reduction method with eco-friendly reduction agent Vitamin C (L (+) ascorbic acid) to fabricate GF (Chua and Pumera, 2014; Ferna'ndez-Merino et al., 2010; Gao et al., 2010; Yousefi et al., 2018; Zhang et al., 2010). Structural morphology of GF is crucial to predict the performance. Here, we used scanning electron microscopy (SEM) to perform the morphology of GF. Although in Fig. 1b there are fluctuations and wrinkles on the surface of GF obviously, the high-magnification SEM image (Fig. 1c) illustrates the detail of the surface still smooth, which could be considered as the results of the re-conjugated of π-π interactions network after Vitamin C successfully removing the oxygen-containing functional groups from graphene oxide sheets (Chen et al., 2016; Liu et al., 2016; Ye et al., 2017). Also, the SEM characterizes the cross-section structure of GF in Fig. 1d, and the fluffy layering pattern is conspicuous. As high-magnification image of Fig. 1e shows, the graphene nanosheets partially delaminated to form the air gaps, which due to the evaporation of water and dissipation of CO, CO_2 from oxygen containing functional group during the heating process. Additionally, the oxalic acids and guluronic acids converted from Vitamin C after reduction might be a factor which prevented agglomerations of graphene nanosheets due to the hydrogen bonds between acids and residual oxygen-containing functional groups available at reduced graphene oxide surfaces (Zhang et al., 2010). These air gaps provide an appreciable out-of-plane compression space, and indicate an excellent piezoresistive performance for pressure sensors.

Meanwhile, 3D optical profiler has been used to explore the waving situation of the GF. As Fig. 1f shows, the fluctuation range is -31.8–31.8 μm, while the thickness of the film is only 25.5 μm. The large scale fluctuation degree presents a great deformability of GF and indicates a sharp resistance decreasing of the GFPS under pressure due to the greatly increase in contact area (Tao et al., 2017). Also, the uniformly distributed fluctuations of peaks and valleys on GF, as Fig. S1 demonstrates as white color area and deep blue color area present in 2D view of optical profile, could provide good uniformity of the pressure sensor devices. Besides, GF exhibits good tensile strength of ~35.31 MPa and excellent elongation of ~5.13% (Fig. S2) which attributes to the air gaps and fluctuations in GF.

To further characterize the GF, XPS technique was used to provide the element count. Fig. 1g shows the XPS survey spectra of graphene oxide film (GOF) and GF, and the intensity ratio of C/O peak increased partially from GOF to GF, indicating the removal of oxygen-containing functional groups in graphene oxide nanosheets. Moreover, the high-resolution C1s core level XPS spectra of GOF and GF in Figs. S3 and S4 present that the in-situ reduction decreased the C-O groups in graphene oxide, and the increase of C(O)O peak in GF could be considered as the residual Vitamin C and side-product acids in reduction process. Additionally, Raman spectra of GF and GOF have been presented in Fig. 1h. Although the spectra present similar shapes of two peaks with D-peak at 1336.11 cm^{-1} and G-peak at 1592.96 cm^{-1}, the intensity ratio of D-peak/G-peak of GF shows slightly increase as compare to GOF. These results above present that the GF is in a moderated reduction degree, which could result a proper large resistance of GF (Chen et al., 2016; Ye et al., 2017; Zhu et al., 2010). Hence, the electrical conductivity of the GF measured by four-probe measurement illustrate a volume conductivity of 27.6 S m^{-1} (detailed information as shown in Table S1 in supplemental information). This mildly large resistance benefits to the measurement of the pressure sensors, because the resistance changing responding to the pressure applied could be considerably large.

3.2. Pressure sensing performance

For a pressure sensor, the sensitivity is one of the most important properties. Here, the sensitivity has been defined by formula $S = \delta(\Delta R/R_0)/\delta P$, where the ΔR is the resistance changing with a certain pressure, R_0 is the initial resistance of GFPS without any pressure, and P refers the pressure applied on GFPS (Pan et al., 2014; Tao et al., 2017). As Fig. 2a demonstrates, the sensitivity of GFPS could be divided to two sections, which coincide with most previously reported pressure sensors (Jian et al., 2017; Tao et al., 2017; Wang et al., 2014), and could be defined as S1 when pressure under 2 kPa and S2 higher than 2 kPa. In the small pressure range of 0–2 kPa, the sensitivity presents an impressive value of 10.39 kPa^{-1}. More importantly, the sensitivity remains to 0.0034 kPa^{-1} in an ultra-wide range up to 200 kPa, which is much wider than most results reported. In addition, the GFPS was successfully tested under 800 kPa pressure, as Fig. S5 shows, and this high-value pressure was harmlessness to our device. Besides, for this ultra-wide operation range pressure sensor, the hysteresis is essential to the performance of the device. As Fig. 2b demonstrates, there are slight hysteresis when pressure lies below 20 kPa, but with the increasing of pressure, there are

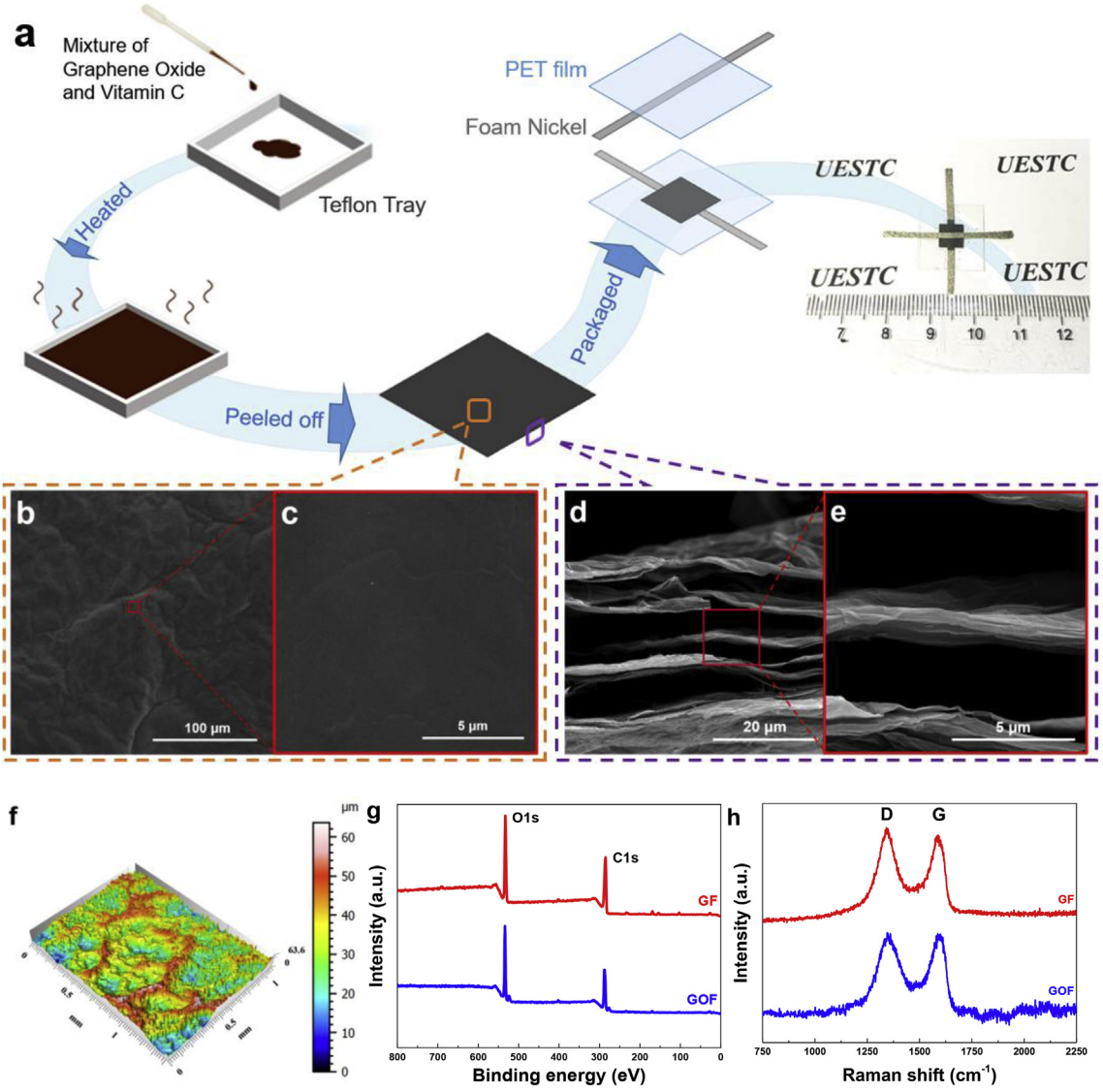

Fig. 1. (a) Fabrication process of GF and GFPS devices. (b) SEM image and (c) high-magnification SEM image of surface of GF. (d) SEM image and (e) high-magnification SEM image of cross-section of GF. (f) 3D topography of GF to demonstrate the fluctuations on surface. (g) XPS survey spectra of GOF and GF. (h) Raman spectra of GOF and GF.

nearly no hysteresis over 60 kPa. This extraordinary performance illustrates advantages of the GF as tactile-sensitive material. Also, the sample-to-sample error of GFPS shows in Fig. 2c. There is nearly no difference among the 6 devices when pressure over 50 kPa and the coefficient of variation (CV) of sample-to-sample variation under any pressure is below 10% (Fig. S6), suggests the good uniformity of the GF in the device.

Furthermore, the durability test under repeated pressure was used to explore the stabilization of GFPS. Fig. 2d demonstrates the response curves of GFPS under 1100 loading-unloading cycles of 20 kPa pressure. From the enlarged plots in Fig. 2d corresponding to 2 cycles at 2000 s, 9000 s and 17150 s respectively, it could be seen that there is no obvious difference between these waves. Importantly, the CV of current response to the repeated applied pressure is 5.10%, which indicates the pressure information could still be perfectly demonstrated by GFPS and the GFPS retains effectiveness and accuracy after cycling pressure applied. These results shows the stableness of the tactile-sensitive structural of GF.

Additionally, for the ultra-wide operation range pressure sensor, the reliability in the full-range is crucial. Hence, as Fig. 2e shows, six different values for 3 kPa, 10 kPa, 20 kPa, 50 kPa, 100 kPa, and 200 kPa of pressure have been applied on GFPS. Obviously, the GFPS presents stable and accord response of the pressure applied and the CV of the response current for the six different pressure are all under 2.5% (as shows in Fig. S7). As the active material, the GF demonstrates impressive effectiveness in the full operation range, and indicates this pressure sensor is perfectly suitable for wide-range detection.

Moreover, the GFPS also presents superb response performance. Fig. 2f demonstrates the response time is 11.6 ms and the recovery time is 25.6 ms, and these results were measured under a pressure of 10 kPa. With these rapid response performance, the GFPS could reach an extremely high working frequency of 5 kPa loading-unloading cycle of 6 Hz, as shown in Fig. 2g.

The overall performance of GFPS is extraordinary among the works reported in the recent 3 years, as Table 1 illustrates. The tradeoff among the four key parameters have slightly decreased sensitivity but significantly enhanced the other three properties, especially the operation range, and presents outstanding performance than other results.

3.3. Discussion of structure-performance dependence

Considering the excellent performance of GFPS, especially the high

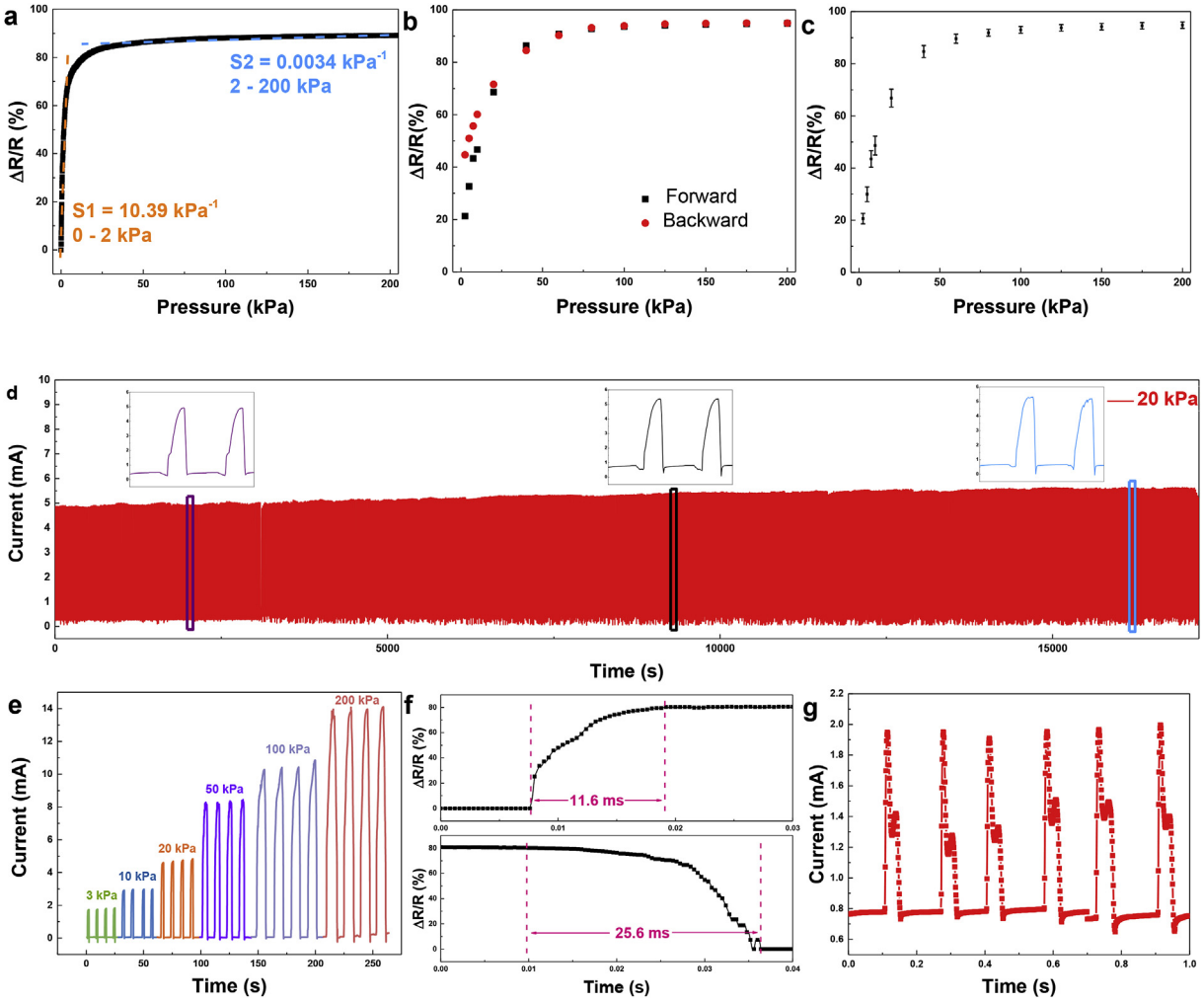

Fig. 2. (a) Resistance changing rate of GFPS response to pressure. (b) The hysteresis of GFPS. (c) The sample-to-sample error plot of GFPS. (d) The current of GFPS corresponding to 1100 cycles of repeated pressure, and enlarged plots corresponding to 2 cycles at 2000 s, 9000 s, and 17150 s, respectively. (e) The current of GFPS response to different repeated pressure. (f) Graphical plots of response (up) and recovery (down) time of GFPS. (g) Plot of GFPS response to 6 Hz of 5 kPa pressure loading-unloading cycle.

Table 1
Comparative analysis of the GFPS with previously reported sensors.

Works	Sensitivity	Operation range	Response time	Durability
Ge et al. (2018)	0.042–0.152 kPa^{-1}	0–27 kPa	96 ms	9000
Liu et al. (2017)	0.4 kPa^{-1}	0–140 kPa	1000 ms	60
Jian et al. (2017)	19.8 kPa^{-1} 0.27 kPa^{-1}	0.6–300 Pa 300–6000 Pa	16.7 ms	35000
Zhang et al. (2018a)	1.71 kPa^{-1} 0.02 kPa^{-1}	0–225 Pa 225–5000 Pa	6 ms	550
Tao et al. (2017)	17.2 kPa^{-1} 0.1 kPa^{-1}	0–2 kPa 2–20 kPa	120 ms	300
This work	10.39 kPa^{-1} 0.0034 kPa^{-1}	0–2 kPa 2–200 kPa	11.6 ms	1100

sensitivity with ultra-wide operation range, it is vital to explore the dependence of material and performance of GFPS. For piezoresistive materials, which reflect pressure information by resistive varying, the performance is determined by conductive structure. In general, there always has been the paradox between high sensitivity and wide operation range for pressure sensors, because high sensitivity demands the easy-deformation ability of the material, but wide-operation range requires good deformation-durability. However, benefited from the air

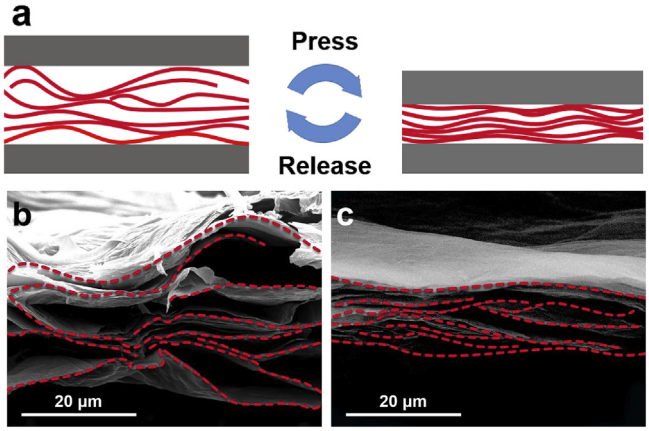

Fig. 3. (a) Schematic illustration of the status of GF in GFPS with and without pressure. (b) Cross-section SEM image of GF without pressure. (c) Cross-section SEM image of GF under pressure.

gaps and fluctuations of GF, the GFPS demonstrated promising performance. As Fig. 3a illustrates, in the initial state without pressure, the GF in the sensor kept its waving surface and fluffy layered structure, and braced the electrodes for a proper height. Once pressure applied, the

contact area between GF and electrodes increased significantly due to the fluctuations faded. Meanwhile, the air gaps inside of GF compressed as well. To confirm the structural deformation situation of GF, SEM were used to illustrate the differences in cross-section of GF with and without pressure. As the SEM images shown, Fig. 3b demonstrates the initial state of GF without pressure, and Fig. 3c demonstrates the status of GF under 10 kPa pressure. Apparently the thickness of GF dramatically decreased from 25.5 μm to 10.9 μm under pressure. These images indicate the decrease of the inter-layer air gaps in GF, and the contact area between graphene sheets increased. Therefore, with the pressure increasing, the contacting between GF and electrodes could be considered as changing from "point-to-face" to "face-to-face" mode, while the contact between graphene sheets changes from "point-to-point" to "point-to-face" and then to "face-to-face" mode (Sheng et al., 2015). Hence, on one hand, the magnificent resistance variation which presenting high sensitivity under small-value pressure could attributed to the co-effect of fluctuations and air gaps. On the other hand, under high pressure, the inter-layer air gaps in GF with the excellent deformation-durability could retain the effectiveness for pressure sensing. The GF proved its structural advantages for pressure sensors, and provide the excellent tactile-sensing performance of the GFPS.

3.4. Application for Traditional Chinese medicine wrist-pulse

With the excellent performance of high sensitivity, ultra-wide operation range, reliable repeatability and impressively rapid response, the tiny-size light-weight GFPS could be used as wearable monitor in biomedical field. Alone with the thousands years history of China, Traditional Chinese medicine (TCM) effectively diagnose diseases and treat patients by inspection, listening and smelling, inquiry and palpation. Especially, the wrist-pulse diagnosis, which using three fingers to feel the pulse at three positions on wrist, is the core of TCM (Luo and Chung, 2016; Ribeiro de Moura et al., 2016; Zhang et al., 2018b). Recording and analyzing the TCM-diagnosing wrist-pulse waveforms could help the doctors to treat patients more conveniently and effectively. Flexible pressure sensors integrated in wearable systems present great potential of monitoring and recording of the wrist-pulse oscillogram, and some researchers successfully shown the waveform measured by flexible pressure sensors (Ge et al., 2018; Gong et al., 2014; Pang et al., 2012). However, flexible pressure sensors reported recently were barely suitable for TCM-diagnosing type wrist-pulse waveforms. One of the reasons is the operation area of traditional flexible pressure sensors is oversized, and the wrist-pulse diagnosis should measure three close-adjacent position synchronously. More importantly, TCM doctor need to apply a pressure by fingertips to diagnose patients' wrist-pulse, and the pressure could over 20 kPa for some patients. Most of flexible pressure sensors lose effectiveness under the pressure of 20 kPa, and the low amplitude wrist-pulse still requires a high-sensitivity measurement.

Here, we demonstrate a practical application of the GFPS for TCM-diagnosing wrist-pulse oscillogram monitoring. As shown in Fig. 4a, three individual GFPS attached on the three different positions named Cun, Guan, Chi of wrist (Luo and Chung, 2016), and connected to adaptation system (more detailed information shows in experimental section in supplemental information) to record the three-channel waveforms of wrist-pulse. When we use fingertips to apply pressure on these three GFPS, the system begins to collect the wrist-pulse information. Fig. 4b presents the three-channel raw signal waveforms without smooth-processing. Obviously, corresponding to the reported results, the Cun waveform shows the largest amplitude, while the Guan waveform is much smaller than Cun, and the Chi waveform has the weakest amplitude (Zhang et al., 2018b). Moreover, attributed to the high sensibility in wide operation range and rapid response, all the three-channel waveforms present three distinct peaks of percussion wave (P-peak), tidal wave (T-peak) and dicrotic wave (D-peak) in every single period with a pulse rate of 80 beats per minute (Ribeiro de Moura et al., 2016; Yang et al., 2018). The tidal wave and dicrotic wave exist in the descending limb of the main percussion wave, which modify the characteristic points of the pulse shape and contain amount of the wrist-pulse information (Wang et al., 2016). Importantly, all the waveforms were measured under around 20 kPa pressure applied on the three position by fingertips, which is same as TCM wrist-pulse measuring by doctors. This wrist-pulse monitoring system with three GFPS shows satisfying performance for TCM wrist-pulse diagnose, and illustrates the great potential in biomedical field.

3.5. Application for bionic fingertip tactile sensing

Importantly, we applied one GFPS on the tip of index finger of the tester for pressure measurement. Firstly, we placed two different counterweights of 20 g and 50 g on one fingertip respectively, and recorded the current/time information. As Fig. 4c demonstrated, the two counterweights were successfully distinguished by GFPS due to the different pressure applied on fingertip and also the waveform plot shows the rapid and sensitive response of GFPS. The GFPS retained its excellent performance and effectiveness in fingertips application. Furthermore, in Fig. 4d, we applied the bionic fingertip tactile sensors for five individual GFPS on the five fingertips of tester's left hand, and connected these GFPS to a real-time display system. This system has been shown in Fig. S8, and could display the pressure value and visualize the pressure-level by color-depth on the screen. Fig. 4e shows a hand in the screen displaying the pressure values in Pa and white block representing no-pressure on fingertips position, and the bottom-right inset illustrates the 5 different intensities of red color corresponding to the 5 levels of exerted pressure. Next, as shown in Fig. 4f, the tester used thumb and index finger to catch a counterweight, and the screen in Fig. 4g displayed the pressure values of the 5 fingertips and color blocks in real-time (Supplementary Movie 1 demonstrates the entire process). It could be seen that the response information of the pressure is rapid and clear, and the GFPS worked in this system stably and efficiently. This system with GFPS on fingertips suggests the excellent tactile-sensing performance and fantastic human-machine interaction ability, illustrating the great application potential in wearable electronics, artificial E-skins and bionic robot. The GFPS confirmed its ability to use as fingertips pressure sensor.

Supplementary video related to this article can be found at https://doi.org/10.1016/j.bios.2019.05.001.

4. Conclusions

In summary, owing to the advanced structure of the GF with fluctuations on surface and fluffy-layered structure in cross-section, the mini-size, light-weight GFPS exhibits promising extraordinary performance. This is the first report of a flexible pressure sensor with the performance of high sensitivity over 10 kPa^{-1} (10.39 kPa^{-1}) along with ultra-wide operation range extend to 200 kPa. Moreover, the GFPS also illustrates impressively stable cyclic stability, high working frequency, rapid response and recovery time. These unique characteristics largely improve the application possibility of GFPS. Meanwhile, the demonstrated results of TCM wrist-pulse detection and bionic fingertip tactile sensors suggest the excellent tactile sensing performance and fantastic human-machine interaction ability of the GFPS. Our GFPS mimics the tactile sensing of fingertips successfully and illustrates the great application potential in biomedical field and bionic skins field.

CRediT authorship contribution statement

Ziyu Yue: Conceptualization, Formal analysis, Writing - original draft, Writing - review & editing. **Xingke Ye:** Writing - review & editing. **Shihong Liu:** Software. **Yucan Zhu:** Writing - review & editing. **Hedong Jiang:** Writing - review & editing. **Zhongquan Wan:** Formal analysis. **Yuan Lin:** Data curation. **Chunyang Jia:** Conceptualization, Project administration, Writing - original draft, Writing - review &

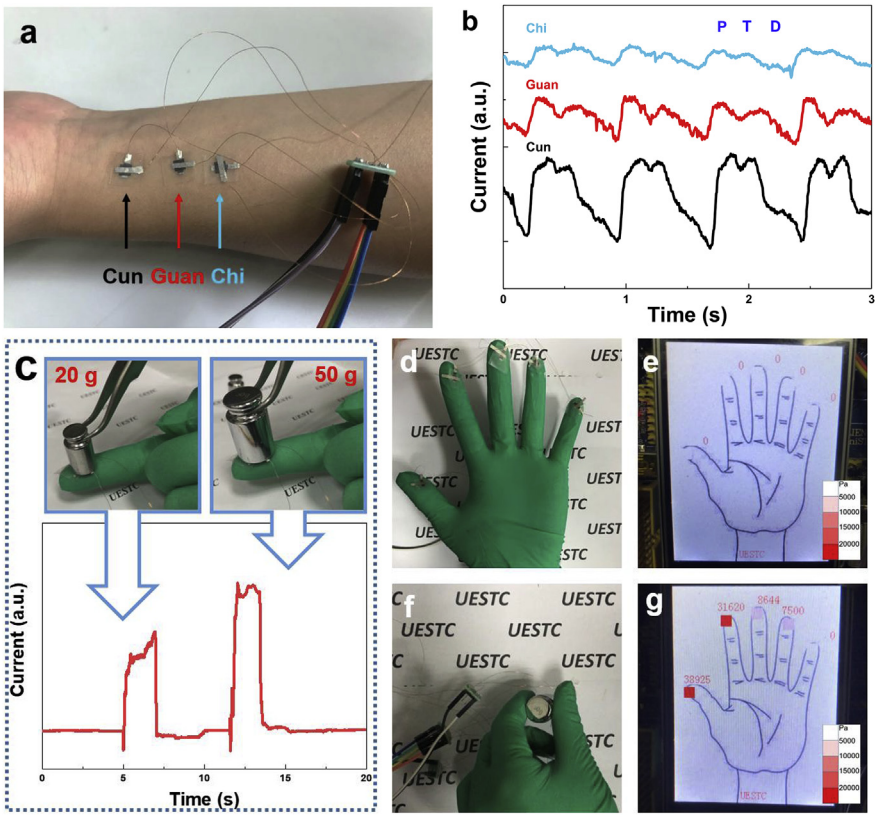

Fig. 4. (a) Photo of three individual GFPS applied on the three position of Cun, Guan and Chi on wrist, and connected to adaption circuits. (b) Plot of the waveform of the three positions detected by GFPS. (c) Response plot of different counterweight applied on fingertip with GFPS. (d) Five individual GFPS applied on fingertips of tester's left hand with no pressure and (e) screen displays pressure value and pressure level by color block. (f) Tester catches a counterweight by thumb and index-finger and (g) screen displays the pressure information. (For interpretation of the references to color in this figure legend, the reader is referred to the Web version of this article.)

editing.

Acknowledgements

We are grateful to the National Natural Science Foundation of China (Grant Nos. 51773027 and 21572030) and National Key R@D Program of China (No. 2017YFB0702800) for financial support.

Appendix A. Supplementary data

Supplementary data to this article can be found online at https://doi.org/10.1016/j.bios.2019.05.001.

References

Ferna´ndez-Merino, M.J., Guardia, L., Paredes, J.I., Villar-Rodil, S., Solı´s-Ferna´ndez, P., Marti´nez-Alonso, A., Tasco´n, J.M.D., 2010. J. Phys. Chem. C 114, 6426–6432.
Chen, X., Meng, D., Wang, B., Li, B.-W., Li, W., Bielawski, C.W., Ruoff, R.S., 2016. Carbon 101, 71–76.
Chen, S., Jiang, K., Lou, Z., Chen, D., Shen, G., 2018. Adv. Mater. Technol. 3, 1700248.
Chou, H.H., Nguyen, A., Chortos, A., To, J.W., Lu, C., Mei, J., Kurosawa, T., Bae, W.G., Tok, J.B., Bao, Z., 2015. Nat. Commun. 6, 8011.
Chua, C.K., Pumera, M., 2014. Chem. Soc. Rev. 43, 291–312.
Gao, J., Liu, F., Liu, Y., Ma, N., Wang, Z., Zhang, X., 2010. Chem. Mater. 22, 2213–2218.
Gao, W., Emaminejad, S., Nyein, H.Y.Y., Challa, S., Chen, K., Peck, A., Fahad, H.M., Ota, H., Shiraki, H., Kiriya, D., Lien, D.-H., Brooks, G.A., Davis, R.W., Javey, A., 2016. Nature 529, 509–514.
Ge, G., Cai, Y., Dong, Q., Zhang, Y., Shao, J., Huang, W., Dong, X., 2018. Nanoscale 10, 10033–10040.
Gong, S., Schwalb, W., Wang, Y., Chen, Y., Tang, Y., Si, J., Shirinzadeh, B., Cheng, W., 2014. Nat. Commun. 5, 3132.
Jian, M., Xia, K., Wang, Q., Yin, Z., Wang, H., Wang, C., Xie, H., Zhang, M., Zhang, Y., 2017. Adv. Funct. Mater. 27, 1606066.
Kim, D., Kim, D., Lee, H., Jeong, Y.R., Lee, S.J., Yang, G., Kim, H., Lee, G., Jeon, S., Zi, G., Kim, J., Ha, J.S., 2016. Adv. Mater. 28, 748–756.
Kim, Y., Chortos, A., Xu, W., Liu, Y., Oh, J.Y., Son, D., Kang, J., Foudeh, A.M., Zhu, C., Lee, Y., Niu, S., Liu, J., Pfattner, R., Bao, Z., Lee, T.-W., 2018. Science 360, 998–1003.
Kuila, T., Bose, S., Khanra, P., Mishra, A.K., Kim, N.H., Lee, J.H., 2011. Biosens. Bioelectron. 26, 4637–4648.
Lai, Y.-C., Ye, B.-W., Lu, C.-F., Chen, C.-T., Jao, M.-H., Su, W.-F., Hung, W.-Y., Lin, T.-Y., Chen, Y.-F., 2016. Adv. Funct. Mater. 26, 1286–1295.
Li, Y., Samad, Y.A., Liao, K., 2015. J. Mater. Chem. A 3, 2181–2187.
Lipomi, D.J., Vosgueritchian, M., Tee, B.C., Hellstrom, S.L., Lee, J.A., Fox, C.H., Bao, Z., 2011. Nat. Nanotechnol. 6, 788–792.
Liu, P., Yang, H., Zhang, X., Jiang, M., Duan, Y., Zhang, J., 2016. Carbon 107, 46–55.
Liu, Y., Tao, L.-Q., Wang, D.-Y., Zhang, T.-Y., Yang, Y., Ren, T.-L., 2017. Appl. Phys. Lett. 110, 123508.
Luo, C.-H., Chung, C.-Y., 2016. Eur. J. Integr. Med. 8, 926–931.
Mannsfeld, S.C., Tee, B.C., Stoltenberg, R.M., Chen, C.V., Barman, S., Muir, B.V., Sokolov, A.N., Reese, C., Bao, Z., 2010. Nat. Mater. 9, 859–864.
Morales-Narvaez, E., Baptista-Pires, L., Zamora-Galvez, A., Merkoci, A., 2017. Adv. Mater. 29, 201604905.
Nesser, H., grisolia, j., Alnasser, T., Viallet, B., Ressier, L., 2018. Nanoscale 10, 10479–10487.
Pan, L., Chortos, A., Yu, G., Wang, Y., Isaacson, S., Allen, R., Shi, Y., Dauskardt, R., Bao, Z., 2014. Nat. Commun. 5, 3002.
Pang, C., Lee, G.Y., Kim, T.I., Kim, S.M., Kim, H.N., Ahn, S.H., Suh, K.Y., 2012. Nat. Mater. 11, 795–801.
Park, H., Kim, D.S., Hong, S.Y., Kim, C., Yun, J.Y., Oh, S.Y., Jin, S.W., Jeong, Y.R., Kim, G.T., Ha, J.S., 2017. Nanoscale 9, 7631–7640.
Park, H., Kim, J.W., Hong, S.Y., Lee, G., Kim, D.S., Oh, J.h., Jin, S.W., Jeong, Y.R., Oh, S.Y., Yun, J.Y., Ha, J.S., 2018. Adv. Funct. Mater. 28, 1707013.
Ribeiro de Moura, N.G., Cordovil, I., de Sá Ferreira, A., 2016. J. Integr. Med. 14, 100–113.
Schwartz, G., Tee, B.C., Mei, J., Appleton, A.L., Kim, D.H., Wang, H., Bao, Z., 2013. Nat. Commun. 4, 1859.
Sheng, L., Liang, Y., Jiang, L., Wang, Q., Wei, T., Qu, L., Fan, Z., 2015. Adv. Funct. Mater. 25, 6545–6551.
Shi, M., Zhang, J., Chen, H., Han, M., Shankaregowda, S.A., Su, Z., Meng, B., Cheng, X., Zhang, H., 2016. ACS Nano 10, 4083–4091.
Tao, L.Q., Zhang, K.N., Tian, H., Liu, Y., Wang, D.Y., Chen, Y.Q., Yang, Y., Ren, T.L., 2017. ACS Nano 11, 8790–8795.
Tian, H., Shu, Y., Wang, X.F., Mohammad, M.A., Bie, Z., Xie, Q.Y., Li, C., Mi, W.T., Yang, Y., Ren, T.L., 2015. Sci. Rep. 5, 8603.
Wang, X., Gu, Y., Xiong, Z., Cui, Z., Zhang, T., 2014. Adv. Mater. 26, 1336–1342.
Wang, D., Zhang, D., Lu, G., 2016. Biomed. Signal Proces. 23, 62–75.
Wang, X., Que, M., Chen, M., Han, X., Li, X., Pan, C., Wang, Z.L., 2017. Adv. Mater. 29, 201605817.
Wang, S., Xu, J., Wang, W., Wang, G.N., Rastak, R., Molina-Lopez, F., Chung, J.W., Niu, S., Feig, V.R., Lopez, J., Lei, T., Kwon, S.K., Kim, Y., Foudeh, A.M., Ehrlich, A., Gasperini, A., Yun, Y., Murmann, B., Tok, J.B., Bao, Z., 2018. Nature 555, 83–88.
Wu, W., Haick, H., 2018. Adv. Mater. 30 201705024.
Yamada, T., Hayamizu, Y., Yamamoto, Y., Yomogida, Y., Izadi-Najafabadi, A., Futaba, D.N., Hata, K., 2011. Nat. Nanotechnol. 6, 296–301.
Yang, Y.F., Tao, L.Q., Pang, Y., Tian, H., Ju, Z.Y., Wu, X.M., Yang, Y., Ren, T.L., 2018. Nanoscale 10, 11524–11530.
Yao, H.B., Ge, J., Wang, C.F., Wang, X., Hu, W., Zheng, Z.J., Ni, Y., Yu, S.H., 2013. Adv.

Mater. 25, 6692–6698.
Ye, X., Zhou, Q., Jia, C., Tang, Z., Zhu, Y., Wan, Z., 2017. Carbon 114, 424–434.
Yousefi, N., Wong, K.K.W., Hosseinidoust, Z., Sorensen, H.O., Bruns, S., Zheng, Y., Tufenkji, N., 2018. Nanoscale 10, 7171–7184.
Zang, Y., Zhang, F., Huang, D., Gao, X., Di, C.A., Zhu, D., 2015. Nat. Commun. 6, 6269.
Zhang, J., Yang, H., Shen, G., Cheng, P., Zhang, J., Guo, S., 2010. Chem. Commun. 46, 1112–1114.
Zhang, J., Zhou, L.J., Zhang, H.M., Zhao, Z.X., Dong, S.L., Wei, S., Zhao, J., Wang, Z.L., Guo, B., Hu, P.A., 2018a. Nanoscale 10, 7387–7395.
Zhang, Z., Zhang, Y., Yao, L., Song, H., Kos, A., 2018b. J. Biomed. Inform. 79, 107–116.
Zhao, S., Zhu, R., 2017. Adv. Mater. 29, 201606151.
Zhu, Y., Murali, S., Cai, W., Li, X., Suk, J.W., Potts, J.R., Ruoff, R.S., 2010. Adv. Mater. 22, 3906–3924.